IEEE Journal of Translational Engineering in Health and Medicine

Received 1 March 2023; revised 7 July 2023 and 11 August 2023; accepted 7 September 2023.
Date of publication 10 October 2023; date of current version 24 November 2023.

Digital Object Identifier 10.1109/JTEHM.2023.3323381

Overground Walking With a Transparent Exoskeleton Shows Changes in Spatiotemporal Gait Parameters

RAFHAEL M. ANDRADE[1,2], (Member, IEEE), STEFANO SAPIENZA[2], ABOLFAZL MOHEBBI[3], (Member, IEEE), ERIC E. FABARA[2], AND PAOLO BONATO[2], (Senior Member, IEEE)

[1]Department of Mechanical Engineering, Universidade Federal do Espirito Santo, Vitória, Espirito Santo 29075-910, Brazil
[2]Department of Physical Medicine and Rehabilitation, Harvard Medical School, Spaulding Rehabilitation Hospital, Charlestown, MA 02129, USA
[3]Department of Mechanical Engineering, Polytechnique Montreal, Montréal, QC H3T 1J4, Canada

CORRESPONDING AUTHOR: R. M. ANDRADE (rafhael.andrade@ufes.br)

This work was supported in part by Fundação de Amparo à Pesquisa e Inovação do Espírito Santo (FAPES) under Project 151/2021, Project 2021-8GJZ6, Project 460/2021, Project 2021-L7SZ4, Project 414/2022, Project 2022-SX1VM, Project 565/2023, Project 2023-BQK22, Project 946/2023, and Project 2023-F0GWQ; in part by Financiadora de Estudos e Projetos (FINEP) com recursos do Fundo Nacional de Desenvolvimento Científico e Tecnológico (FNDCT) under Grant 2784/20; in part by Coordenação de Aperfeiçoamento de Pessoal de Nível Superior (CAPES) (finance Code 001); and in part by the Peabody Foundation.

This work involved human subjects or animals in its research. Approval of all ethical and experimental procedures and protocols was granted by the Institutional Review Board of Spaulding Rehabilitation Hospital.

ABSTRACT Lower-limb gait training (GT) exoskeletons have been successfully used in rehabilitation programs to overcome the burden of locomotor impairment. However, providing suitable net interaction torques to assist patient movements is still a challenge. Previous transparent operation approaches have been tested in treadmill-based GT exoskeletons to improve user-robot interaction. However, it is not yet clear how a transparent lower-limb GT system affects user's gait kinematics during overground walking, which unlike treadmill-based systems, requires active participation of the subjects to maintain stability. In this study, we implemented a transparent operation strategy on the ExoRoboWalker, an overground GT exoskeleton, to investigate its effect on the user's gait. The approach employs a feedback zero-torque controller with feedforward compensation for the exoskeleton's dynamics and actuators' impedance. We analyzed the data of five healthy subjects walking overground with the exoskeleton in transparent mode (ExoTransp) and non-transparent mode (ExoOff) and walking without exoskeleton (NoExo). The transparent controller reduced the user-robot interaction torque and improved the user's gait kinematics relative to ExoOff. No significant difference in stride length is observed between ExoTransp and NoExo ($p = 0.129$). However, the subjects showed a significant difference in cadence between ExoTransp (50.9 ± 1.1 steps/min) and NoExo (93.7 ± 8.7 steps/min) ($p = 0.015$), but not between ExoTransp and ExoOff ($p = 0.644$). Results suggest that subjects wearing the exoskeleton adjust their gait as in an attention-demanding task changing the spatiotemporal gait characteristics likely to improve gait balance.

INDEX TERMS Lower-limb exoskeleton, gait training, transparent control, gait kinematics.

I. INTRODUCTION

Gait training (GT) exoskeletons are extraordinary tools used in lower-limb rehabilitation that can provide specific, intensive and task-oriented therapies for several impairments [1]. GT lower-limb exoskeletons can be divided in two main groups: treadmill-based GT and overground GT robot-assisted systems [2]. The former employs a lower-limb exoskeleton assembled in a structure over a treadmill, such as Lokomat® (Hocoma AG, Switzerland) and ALEX [3]. In such a system, body-weight support and handrails are used to stabilize the user and prevent falls. On the other hand, in overground GT exoskeletons, such as HAL

IEEE Journal of Translational Engineering in Health and Medicine

(Cyberdyne Inc., Japan) [4], Ekso (Ekso Bionics, USA) [5] and many others [6], the users have to adjust their gait and balance to the system dynamics. Despite the achievements in lower-limb rehabilitation with treadmill-based robotic GT [7], this approach aims at feedforward control of lower-limb movements and has limited impact on the volitional control of gait that occurs when the subject's balance is challenged [8]. Instead, overground GT exoskeletons have the advantage of facilitating the achievement of physiological gait patterns while challenging the balance control system [9], thus improving the benefits of rehabilitation.

Active participation of the user in rehabilitation robotics has been shown to be crucial to better outcomes [10]. Different compliant control strategies were proposed in gait rehabilitation following the assistance-as-needed (AAN) concept [11]. Active impedance control and its variants [12], [13], [14] and the teleimpedance approach [15] are some examples. Despite the achieved outcomes, these techniques face limitations in generating suitable net user-robot interaction forces due to the weight and inertia of the system and poor backdrivability of the actuators. In this direction, an ideal AAN GT system must display highly transparent motion to the user and produce torque only when the voluntarily-generated motor output deviates significantly from the physiological trajectory [16]. However, transparency is still an open problem in wearable-robots [17]. The system adds mechanical impedance to the legs and constraints to the joints preventing the user moving at will.

Strategies to improve transparency in robotic devices have been addressed as mechanical and control approaches among research groups [18]. In general, to reduce unwanted user-robot interaction forces, the weight and inertia of the overall system must be minimized, and the actuators have to be backdrivable and kinematic compatible with the user joints [19]. However, there is a trade-off between actuators' backdrivability and weight. Greater backdrivablility can be achieved with direct or quasi-direct drive actuators [20] composed of high-torque low-speed DC motors integrated with gearboxes with low reduction ratio, but this design usually results in heavy and bulky actuators. On the other hand, lightweight actuators composed of low-torque and high-speed DC motors associated with high reduction ratio gearboxes, e.g., harmonic drives, are marked by high friction and apparent inertia, thus limiting their operation in the reverse direction, that is, low backdrivability [21]. To overcome the drawbacks of low backdrivable actuators, clutches were used between the actuator's output and load [22], [23], [24], but this approach increases the overall weight of the system. Moreover, mechanical constraints and number of degrees-of-freedom (DoF) of the exoskeleton also play a role on the robot's transparency [25]. In an attempt to investigate the effects of the mechanical structure and design elements of an exoskeleton on the user's gait, Bartenbach et al. [26] designed a passive lower limb research platform with kinematic compatible joints. Users experienced reduced step height and increased step length when wearing the exoskeleton platform, in treadmill walking experiments.

From the control point of view, different strategies were proposed over the years to improve user-robot physical interaction. Vallery et al. [27] presented a patient-cooperative control strategy based on generalized elasticities to reduce the physical interaction between robot and human. The authors observed lower cadence and an increase in step length with the proposed transparent method in treadmill experiments. Zanotto et al. [3] experimented a zero-impedance controller with interaction force/torque sensor between the robot and the user's leg in the ALEXII treadmill-based exoskeleton. The proposed method could reduce the user-robot interaction torque and improve the gait kinematics of the user. Chen et al. [28] and Claros et al. [29] achieved high backdrivability in knee joint exoskeletons. The former proposed an adaptive identification method of human motor intent based on EMG input signal, and the latter used force-sensing resistors (FSR) to monitor user-robot interaction and detect user's intention of motion. Both proposed methods were validated in experiments with a standing subject moving the knee.

Despite the advances of the methods mentioned above to improve transparency in treadmill-based systems, the effects of a transparent overground GT lower-limb exoskeleton on the user's gait are not yet clear. In this study, we investigated gait kinematics and spatiotemporal parameters of five healthy subjects while walking on level ground with the ExoRoboWalker, a six DoF lower-limb exoskeleton designed for gait training.

II. METHODOLOGY

A. EXPERIMENTAL SETUP

The ExoRoboWalker, Fig. 1, is a six degrees-of-freedom lower-limb exoskeleton for overground GT designed to assist movements of the hip, knee, and ankle of both legs in the sagittal plane. The exoskeleton is composed by six harmonic drive-based actuators, consisting of an EC 45 flat 70W brushless motor (Maxon Motors, Switzerland) and a CSD-20-2a harmonic drive, ratio of 160 (Harmonic Drive LLC, USA). Lateral bars in aluminum link the actuators to footplates with sensorized insoles and lumbar support and to the user's legs by cuffs placed on the thigh and shank. Potentiometers are mounted on each actuator to measure joint angles and to derive angular velocity and acceleration. User-robot interaction torques are measured by strain gauges arranged in a full Wheatstone bridge used as torque sensor attached to each joint. Two FSRs in each insole detect the gait phase. All sensors communicate with the control hardware through a CAN BUS. The core of the control architecture is a PC104 computer that runs a Matlab kernel with real-time control capabilities. The control algorithms are implemented using Simulink under the xPC Target module [9]. The main controller, motor drivers and power supply are set on a ceiling -mounted hoist to reduce the overall weight bared by the user and to allow for free movement during overground walking.

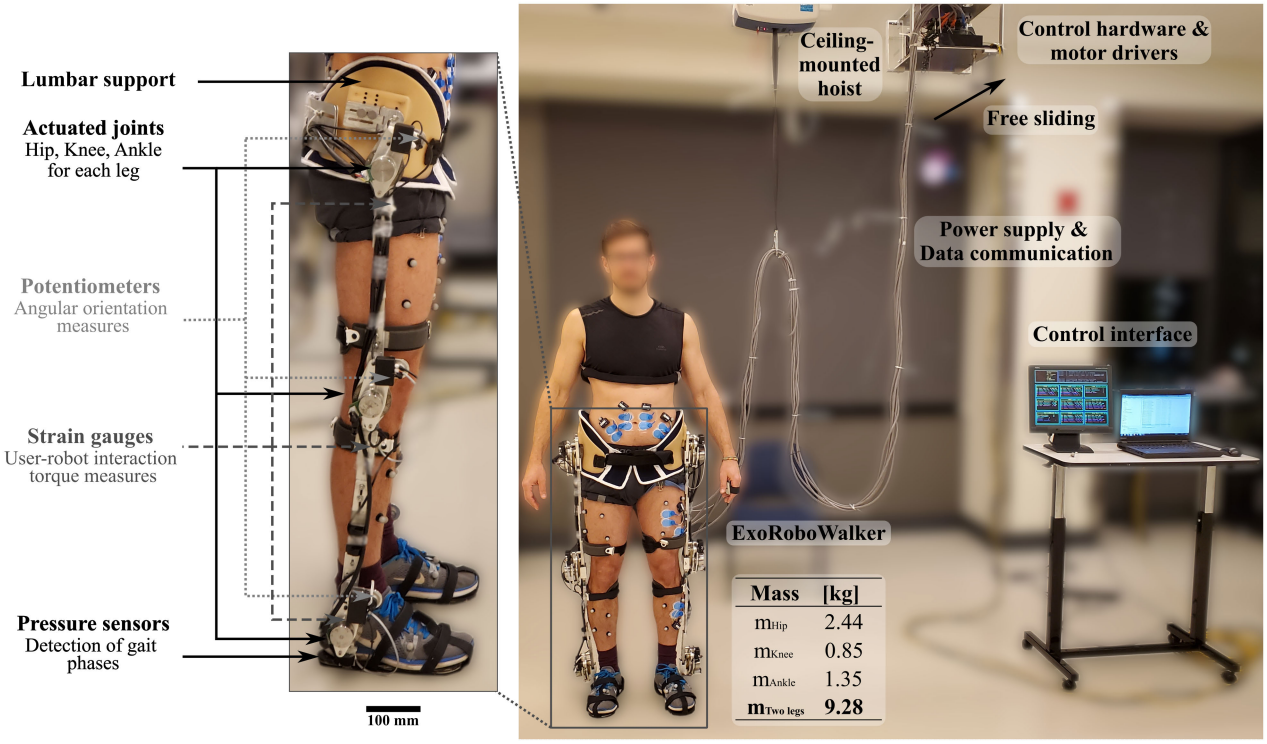

FIGURE 1. The experiment setup consists of a six degree-of-freedom lower-limb exoskeleton with control hardware and power supply set on a ceiling-mounted hoist allowing for reduced overall weight of the system and free movement during overground walking. The control interface allows the therapist to set the control parameters of the system and provides quantitative feedback on the ability of the patient to ambulate. The ExoRoboWalker mechanics is composed of six harmonic drive-based actuators mounted on the hip, knee and ankle joints, lateral bars between actuators, lumbar support, and insoles. The sensing consists of strain gauges to measure user-robot interaction torques, a potentiometer in each joint, and two pressure sensors on each of the insoles.

The control interface allows the therapist to set the control parameters of the system and provides quantitative feedback on the ability of the patient to ambulate.

B. EXOSKELETON DYNAMICS COMPENSATION

To avoid the effects of the exoskeleton's dynamics on the user-robot interaction, the inertial, Coriolis, centrifugal and gravitational forces should be properly canceled. Double-pendulum is a simple physical system that can display complex dynamics and is the most used model to compute the dynamic effects of lower-limb exoskeletons [30]. Ideally double-pendulum consists of two links l_1 and l_2 with masses m_1 and m_2 that connect two joints with angles θ_1 and θ_2, respectively. As the ExoRoboWalker actuators are centered on the joints and the lateral bars are lightweight, we assume that the double-pendulum model has weightless links and masses m_1 and m_2, corresponding to the actuator mass, concentrated at the end of the links l_1 and l_2, respectively [17]. In this direction, the robot's equation of motion can be expressed as:

$$\tau_{dyn} = M(\theta)\ddot{\theta} + C\left(\theta, \dot{\theta}\right)\dot{\theta} + G(\theta) \tag{1}$$

where τ_{dyn} is the required torque to move the joints, θ is the vector of relative angles of the links l_1 and l_2, θ_1 and θ_2 respectively, M is the mass matrix (2), C is the Coriolis and centrifugal matrix (3), G is the gravitational matrix (4).

$$M = \begin{bmatrix} (m_1+m_2)\,l_1^2 + \cdots & -m_2\left(l_1 l_2 \cos\theta_2 + l_2^2\right) \\ +m_2\left(2l_1 l_2 \cos\theta_2 + l_2^2\right) & m_2 l_2^2 \\ -m_2\left(l_1 l_2 \cos\theta_2 + l_2^2\right) & \end{bmatrix} \tag{2}$$

$$C = \begin{bmatrix} -2m_2 l_1 l_2 \sin\theta_2 \dot{\theta}_2 & m_2 l_1 l_2 \sin\theta_2 \dot{\theta}_2 \\ m_2 l_1 l_2 \sin\theta_2 \dot{\theta}_1 & 0 \end{bmatrix} \tag{3}$$

$$G = \begin{bmatrix} (m_1+m_2)\,l_1 g \sin\theta_1 + m_2 l_2 g \sin(\theta_1 - \theta_2) \\ -m_2 l_2 g \sin(\theta_1 - \theta_2) \end{bmatrix} \tag{4}$$

Considering the overground gait, during the swing phase, the system is designed as a hanging double pendulum with the hip as a fixed point, so that $m_1 = m_{\text{Knee}}$, $m_2 = m_{\text{Ankle}}$, $l_1 = l_{\text{Thigh}}$, $l_2 = l_{\text{Shank}}$, $\theta_1 = \theta_{\text{Hip}}$ and $\theta_2 = \theta_{\text{Knee}}$. During the stance phase, the model assumes the inverted double pendulum configuration, with the ankle joint as a fixed point and $m_1 = m_{\text{Knee}}$, $m_2 = m_{\text{Hip}}$, $l_1 = l_{\text{Shank}}$, $l_2 = l_{\text{Thigh}}$, $\theta_1 = \theta_{\text{Ankle}}$ and $\theta_2 = \theta_{\text{Knee}}$.

C. ACTUATOR DYNAMICS COMPENSATION

Even with the exoskeleton dynamics properly canceled, the actuators remain a substantial source of impedance, mainly due to the harmonic drive-based actuators that are characterized by high friction and low backdrivability [31].

IEEE Journal of Translational Engineering in Health and Medicine

The dynamic model of the actuator, considered as an isolated unit, computes inertia, damping, and stiffness as follows:

$$\tau_{act} = J_e\ddot{\theta} + \tau_f\left(\dot{\theta}, \dot{\theta}_s, \tau_c, \tau_s, b\right) + k\theta \tag{5}$$

where J_e is the equivalent inertia of the actuator ($J_e = 0.745$ kg.m^2) and can be calculated by (6), where $J_m = 1.81$E-05 kg.m^2 is the inertia of the motor's rotor and $J_G = 9.00$E-06 kg.m^2 is the HD gearbox inertia, as provided by the manufacturer. $J_a = 2.0$E-06 kg.m^2 is the gearbox adapter inertia and $N = 160$ is the HD transmission ratio.

$$J_e = (J_m + J_G + J_a)\,N^2 \tag{6}$$

Since non-elastic elements are used in the actuators, the term $k\theta$ is disregarded from the dynamic model. Lastly, τ_f represents the damping force created by the internal friction of the actuator and is a key aspect to improve the system's backdrivability. Usually, robotic actuators are characterized by high ratio transmission enabled by harmonic drives [9], [22], ball screws [5] or planetary gears [20] that create stick-slip behavior during backdrive operation. In this context, just considering the viscous friction [32] or the Coulomb friction-based models [3], [16], on the actuator dynamics would not be a good approach. The torques and angular velocities experienced by the joints are quite different during the stance and swing phases [22]. In addition, the friction forces resulting from direct and reverse joint operation are significantly different, especially in harmonic drive-based actuators [33], [34]. Considering that, we used here a friction model (7), based on the Lund-Grenoble (LuGre) dynamic friction model [35], that considers steady state friction characteristics, such as Coulomb and viscous friction, integrated with the Stribeck effect and stiction friction.

$$\tau_f = \tau_C + \sigma\dot{\theta} + (\tau_S - \tau_C)\,e^{-\left(\frac{\dot{\theta}}{\dot{\theta}_s}\right)^2} \tag{7}$$

where τ_C is the Coulomb friction force, σ is the viscous friction coefficient, τ_S is stiction friction force and $\dot{\theta}_s$ is the Stribeck velocity.

The friction model parameters, presented in TABLE 1, were experimentally fine-tuned for each joint of the exoskeleton. The joint was disconnected from the other components of the exoskeleton to avoid inertial and dynamic torques. We measured the required torque necessary to move the joints at nine different angular velocities ranging from 0 to 1 rad/s. The experiments were carried out in constant angular velocity using a PI velocity controller. The steady state friction torque parameters were calculated by minimizing the squared error between the measured torque and the friction model (7). The results are shown in Fig. 2. Although the measured friction torque denoted by the squares has a high variability (vertical bars), mainly in greater angular velocities, the proposed friction model (solid line) could satisfactorily match the friction behavior of the actuator.

TABLE 1. Optimized parameters of the friction model.

Joint	Parameter	Value
Hip	τ_c	2.91 [N m]
	τ_s	4.2 [N m]
	$\dot{\theta}_s$	0.01 [rad/s]
	σ	6.99 [Nms/rad]
Knee	τ_c	2.24 [N m]
	τ_s	2.94 [N m]
	$\dot{\theta}_s$	0.01 [rad/s]
	σ	4.49 [Nms/rad]
Ankle	τ_c	2.65 [N m]
	τ_s	4.40 [N m]
	$\dot{\theta}_s$	0.02 [rad/s]
	σ	4.45 [Nms/rad]

D. TRANSPARENT OPERATION CONTROL LOOP

The proposed transparent operation control loop is based on a PD zero-torque controller integrated with two feedforward branches to compensate the dynamics of the exoskeleton and actuators. The overview of the proposed controller is depicted in Fig. 3. The physical human-robot interaction (τ_{HRI}) is gathered from the torque sensors of each joint and used as feedback in the zero-torque controller. The signal is properly subtracted from τ_{dyn} to cancel the effects of the exoskeleton dynamics on the measured torques ($\tau_{\text{HRI}} = \tau_{\text{sensor}}$-$\tau_{\text{dyn}}$). τ_{act} is computed according to Eq.(5). To avoid false actuation, thresholds for $\dot{\theta}$, $\ddot{\theta}$ and t_{HRI} are used in the actuator compensation branch. Just if $\ddot{\theta}$ is greater than $\ddot{\theta}_{min}$, the inertial term is computed for τ_{act}. The friction term (Eq.(7)) is considered if $\tau_{\text{HRI}} > \tau_{\text{HRImin}}$ and $\dot{\theta} > \dot{\theta}_{min}$, but if $\tau_{\text{HRI}} > \tau_{\text{HRImin}}$ and $\dot{\theta} < \dot{\theta}_{min}$ then $\tau_{\text{f}} = \tau_{\text{S}}$. Hence, τ_{act} and τ_{dyn} are added to the zero-torque controller output before τ_{cont} being sent to the joints.

The proposed controller requires a total of eight tuned parameters for each joint to improve the transparency of the system, as presented in TABLE 2. Although sophisticated methods based on genetic algorithms or particle swarm optimization algorithms were previously proposed to optimize the control parameters of exoskeletons [36], our system cannot use such approaches. Firstly, since the control system is based on minimizing the user-robot interaction, the parameters should be tuned as the user moves while wearing the exoskeleton. The actuators should have quick and stable response, but not cause instabilities among joints. Finally, the tuned system must be stable to avoid generating perturbations, that could possibly cause falls. Due to these safety issues, the parameters had to be empirically tuned.

With the exoskeleton in standing position, we executed an input step-up and step-down of about 90° (hip and knee joints) and 20° (ankle joint) in 1,5s to simulate the motion and frequency of the legs during walking. The parameters were smoothly adjusted step by step to minimize the interaction torque and avoid oscillations between joints. The angular velocity of the ankle joint was found to be very sensitive to

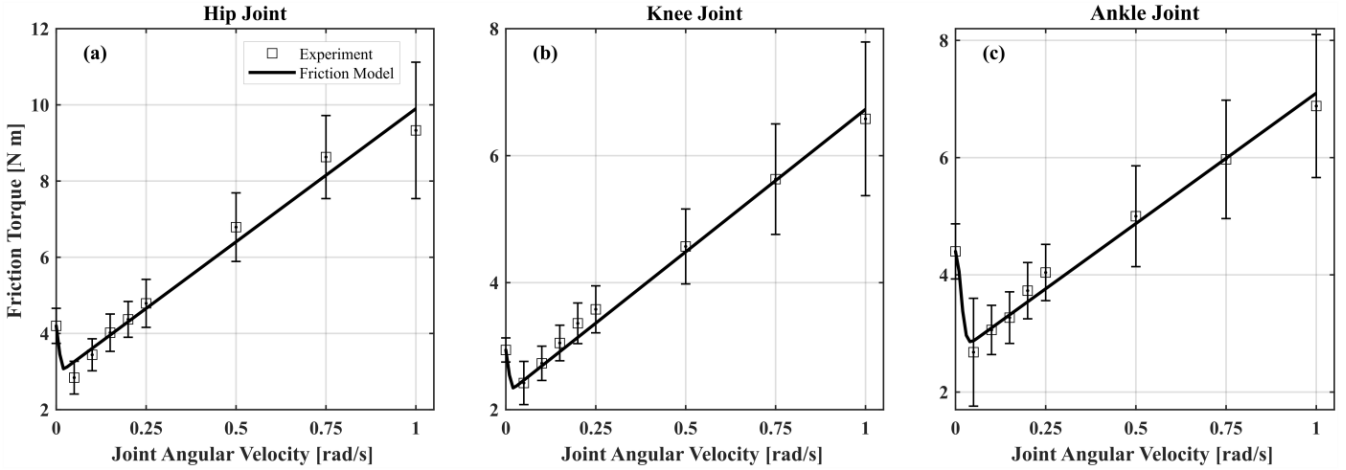

FIGURE 2. Frictional torque vs. angular velocity for hip (a), knee (b), and ankle (c) joints. Squares represent the measured torque required to rotate the joint, vertical bars are the standard deviation, and the black solid lines are the adjusted friction model considering Coulomb and viscous friction, with Stribeck effect and stiction friction.

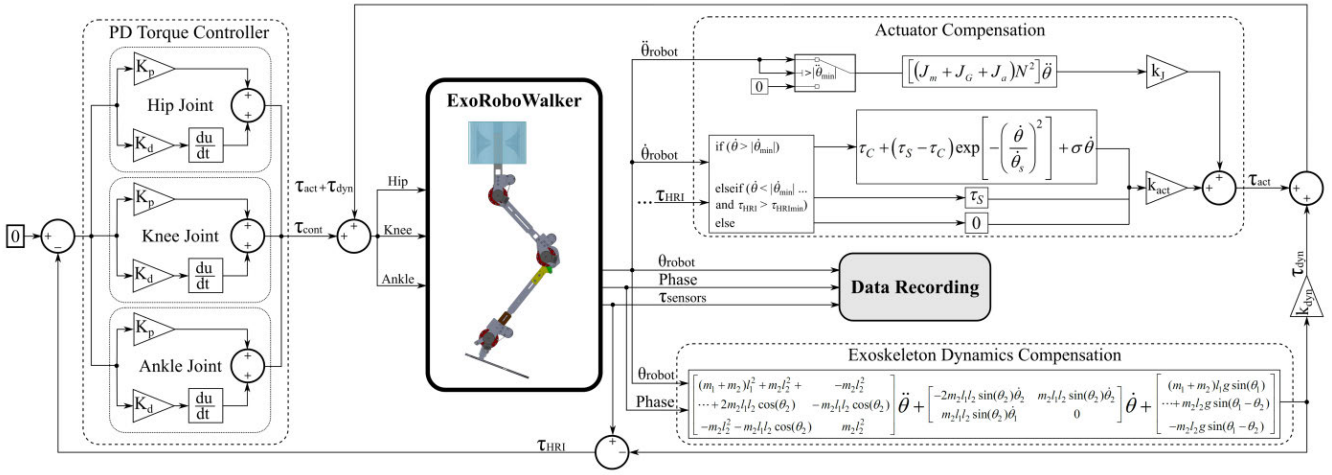

FIGURE 3. ExoRoboWalker control loop for transparent operation consisting of a feedback zero-torque controller based on the user-robot interaction torque (τHRI) of each joint. Two feedforward control branches are used to cancel the effects of the actuator impedance, according to Eqs. (5) to (7), and the exoskeleton dynamics, according to Eqs. (1) to (4).

the variation of these parameters. As the foot has the function of contacting the ground and supporting the body weight, especially during the single support phase, it is desirable that this joint provides greater impedance to increase gait stability with the exoskeleton [5], [6]. Therefore, reduced compensation was applied to the ankle joint to increase stability, especially during heel strike and toe off. The angle and torque responses and the adjusted parameters of the tuned system are presented in Fig. 4 and TABLE 2, respectively. The maximum interaction torque to perform the movement is about 5 N m (hip and knee joints) and about 3 N m (ankle joint), as shown in Fig. 4. It is worth mentioning that with the exoskeleton unpowered we could not easily overcome the exoskeleton joint impedance. Hence, no data is shown here in the unpowered condition. Once the system was tuned, the parameters presented in TABLE 2 were used in the experiments labeled as ExoTransp.

E. EXPERIMENT PROTOCOL

Five adult subjects, four male and one female (72.2 $\pm$ 12.1 kg, 1.76 $\pm$ 0.04 m and 29.4 $\pm$ 5.1 years) were asked to walk on level ground at self-selected gait speed with the ExoRoboWalker. Subject's parameters (leg length, pelvis angle and mass) were used to tune the system before starting the data collection. The subjects walked with the motors of the exoskeleton unpowered, these results were labeled ExoOff, and with the exoskeleton working with the proposed transparent operation, labeled ExoTransp. The ExoOff results were used as a reference for comparison to evaluate the gait kinematics of the subject with the proposed transparent controller. To avoid biased results, the ExoOff and ExoTransp conditions were tested in random order. The ceiling-mounted hoist that we used in the study covered an area of 8 m $\times$ 3 m; thus, for gait analysis, we analyzed gait cycles observed over a span of 6 m. For each mode of operation, a set

IEEE Journal of Translational Engineering in Health and Medicine

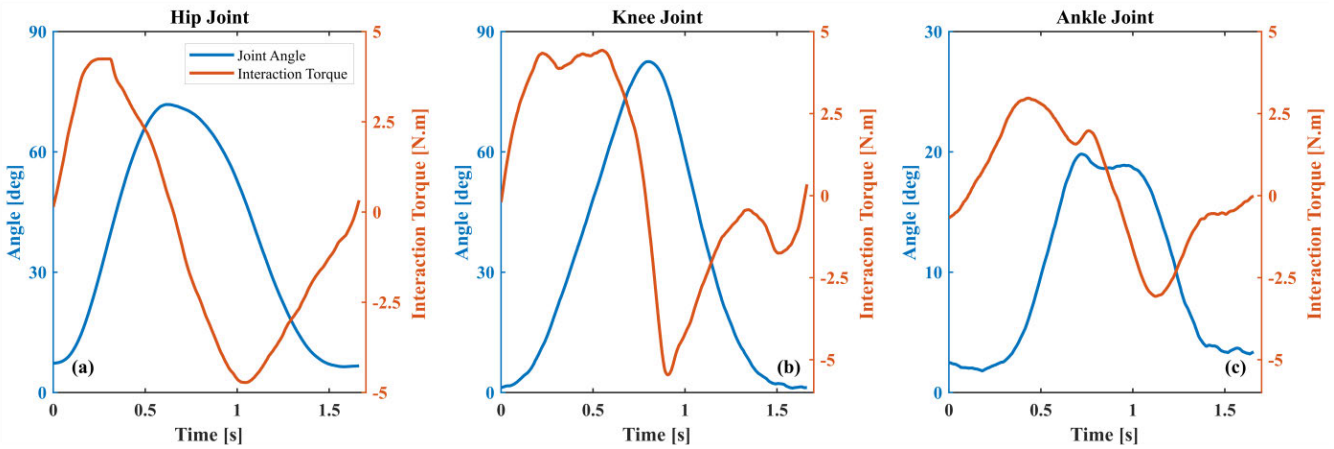

FIGURE 4. Average joint angle and interaction torque for the hip (a), knee (b), and ankle (c) joint for a step-up/down angle input experiment with duration of about 1.5 s. The blue lines represent the joint angles, and the orange lines are the interaction torques. The max interaction torque is about 5,0 N m (hip and knee joints) and 3.0 N m (ankle joint) to perform the movement.

TABLE 2. Tuned parameters of the control system.

Joint	Parameter	Value
Hip	K_p	2.0
	K_d	0.05
	$\ddot{\theta}_{min}$	0.3 [rad/s²]
	$\dot{\theta}_{min}$	0.1 [rad/s]
	τ_{HRImin}	0.3 [N m]
	k_J	0.1
	k_{act}	0.7
	k_{dyn}	0.6
Knee	K_p	5.0
	K_d	0.05
	$\ddot{\theta}_{min}$	0.3 [rad/s²]
	$\dot{\theta}_{min}$	0.1 [rad/s]
	τ_{HRImin}	0.3 [N m]
	k_J	0.1
	k_{act}	0.9
	k_{dyn}	0.6
Ankle	K_p	1.0
	K_d	0.1
	$\ddot{\theta}_{min}$	0.3 [rad/s²]
	$\dot{\theta}_{min}$	0.1 [rad/s]
	τ_{HRImin}	0.3 [N m]
	k_J	0.1
	k_{act}	0.6
	k_{dyn}	0.6

of 4 trials of 6 meters was performed before the data recording. This allowed the users familiarize themselves with the system. Preliminary experiments showed that 30 steps, or approximately 15 meters of walking, were enough for the user to get used to the system. After that, two trials of 6 meters were recorded for gait analysis. Rest breaks were given between sets to avoid fatigue effect in the results. A therapist pulled the ceiling mounted hoist. Finally, after these trials, all subjects doffed the exoskeleton, rested for 5 minutes, and freely walked; this data collection was named NoExo.

Angular and spatiotemporal data were collected using a ten-infrared camera motion analysis system (Vicon, Oxford, UK) with a 1.0 kHz sampling frequency. Markers were placed on anatomical landmarks of the subject's lumbar region, pelvis, thigh, shank, and foot. The user-robot interaction torque was recorded by the torque sensors of each joint with 500 Hz sampling frequency. The signal was low-pass filtered using an elliptic filter. The experimental protocol was approved by the Institutional Review Board of Spaulding Rehabilitation Hospital. Subjects signed an informed consent form to participate in the study. All study procedures were carried out in accordance with all relevant guidelines and regulations.

F. STATISTICAL ANALYSIS

Statistical analyses were performed to evaluate differences between testing conditions. Main outcome measures such as joint angles, interaction torques, RMS interaction torques, step height and step length were evaluated using means and standard deviations. Comparisons of the spatiotemporal parameters (cadence, stride length, step height and gait speed) and temporal parameters (% stance phase, % toe off, % single support and % double support phases) of the gait cycle were performed with paired samples t-test with significance set at 0.05. The data presented normal distributions, verified with the Shapiro-Wilk test for small samples. The null hypothesis ($p > 0.05$) assumes that there is no statistically significant difference between the true mean of the paired samples. The alternative hypothesis assumes that the true mean difference between the paired samples is not equal to zero ($p < 0.05$).

III. RESULTS

The main objective of this study is to assess the effects of a transparent lower-limb exoskeleton on the gait kinematics of healthy subjects during overground walking. The data shown here represents the results of five healthy subjects walking with the ExoRoboWalker in ExoOff and ExoTransp

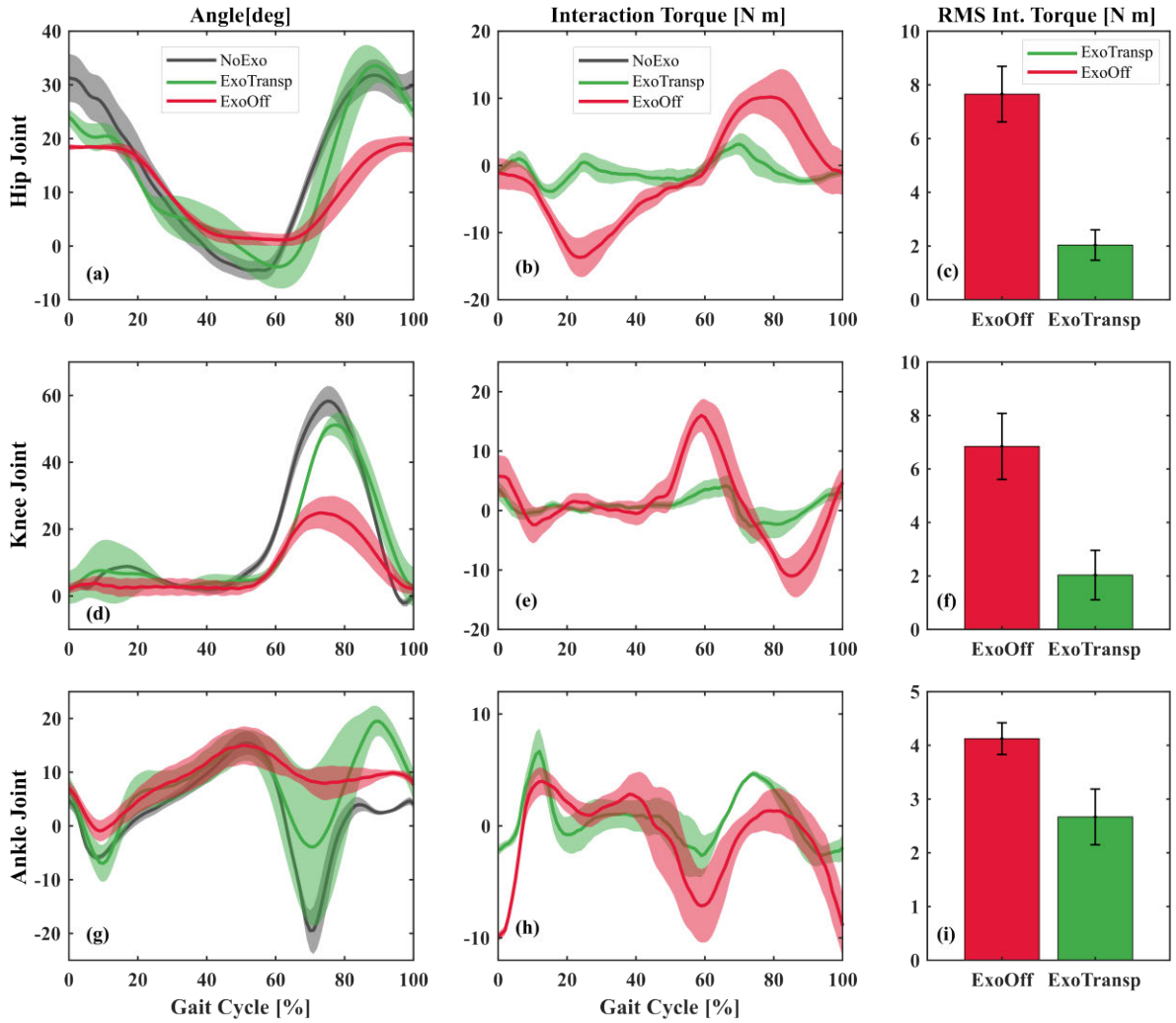

FIGURE 5. Joint angles (hip (a), knee (d) and ankle (g)) and interaction torques (hip (b), knee (e) and ankle (h)) during over-ground walking with the exoskeleton unpowered (red), working in transparent mode (green) and without exoskeleton (gray). RMS interaction torque for hip (c), knee (f) and ankle (i) joints during a gait cycle. The solid lines are the average values. The shaded areas and vertical bars are the variability of the parameter computed as standard deviation.

operating modes and walking with no exoskeleton, NoExo, as a reference for comparing results. To investigate the gait kinematics of the subjects under those different conditions, we first report the joint angles and human-robot interaction torques as a function of the gait cycle. Secondly, the output of the proposed transparent controller is presented. Next, the range of motion (RoM) of the hip and knee joints and heel trajectory are reported to investigate foot clearance. Finally, to assess the effects of the transparent controller on the spatiotemporal parameters of the gait, we performed some statistical analyses for ExoOff, ExoTransp, and NoExo conditions considering stride length, step height, and others as independent variables.

Joint angles and human-robot interaction torque during the gait cycle are presented in Fig. 5. In Fig. 5(a), (d) and (g) are depicted the angles of the hip, knee, and ankle joints, respectively. The red line represents the angles achieved with ExoOff mode, while the green lines are the results of ExoTransp mode, and the gray lines are the angles of the joints for the free walking mode, NoExo. Solid lines are the average values, and shaded areas are the variability of the parameter computed as standard deviation. Compared to the ExoOff results, the average values (solid line) of the hip, knee and ankle joints angles present greater RoM while the user walks with the exoskeleton set as ExoTransp. The average ExoTransp ankle angle is almost the same as the NoExo one, except for the overshoot in the dorsiflexion angle after the toe-off. Even with reduced compensations to increase joint impedance, the ankle angle shows high variance while in ExoTransp mode.

Human-robot interaction torque (τ_{HRI}) is measured at the hip, knee and ankle joints as shown in Fig. 5(b), (e) and (h), respectively. Compared to the ExoOff mode, the averages τ_{HRI} are substantially reduced in ExoTransp trials (solid green

IEEE Journal of Translational Engineering in Health and Medicine

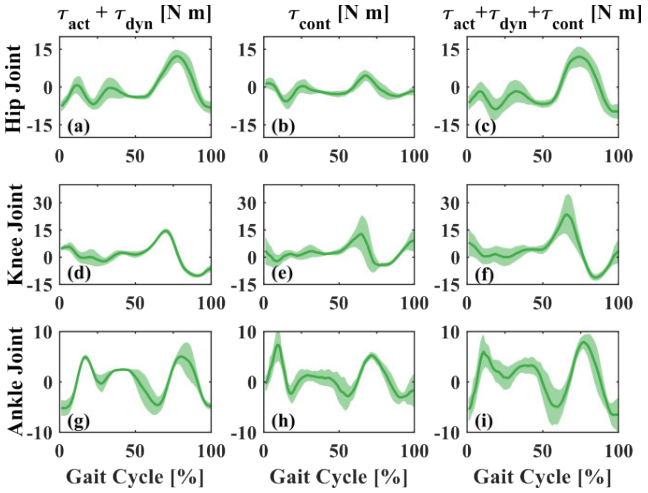

FIGURE 6. Actuator and dynamic compensation ($\tau_{act} + \tau_{dyn}$) (left), zero-torque controller output (τ_{cont}) (middle) and total torque commanded to the actuators ($\tau_{act} + \tau_{dyn} + \tau_{cont}$) (right) during over-ground walking for hip (top), knee (middle) and ankle (bottom) joints. Solid green lines represent the average of the parameters for the exoskeleton in transparent mode. The shaded areas represent the variability (i.e., standard deviation).

lines), mainly for hip and knee joints. The average τ_{HRI} reached picks of 13.8, 16.1 and 9.6 N.m, respectively in the hip, knee and ankle joints during ExoOff and no more than 3.8, 4.1 and 6.5 N m for Exotransp. The difference in τ_{HRI} between ExoOff and ExoTransp trials can be better observed with the RMS value of τ_{HRI} during the gait cycle, as shown in Fig. 5(c), (f), and (i). The average RMS τ_{HRI} for hip, knee, and ankle joints are 7.8, 6.7 and 4.2 for ExoOFF and 2.0, 2.1 and 2.5 for ExoTransp, respectively.

Compensations applied to cancel the effect of the actuator dynamics and the exoskeleton structure dynamics in addition to the output torque of the zero-torque controller are shown in Fig. 6. Fig. 6(a), (d) and (g) depicts $\tau_{act} + \tau_{dyn}$, i.e., the total feed-forward torque compensation. Fig. 6 (b), (e) and (h) present the output of the zero-torque controller for the hip, knee, and ankle joints, respectively. The total torque generated by the hip (Fig. 6(c)) knee (Fig. 6(f)) and ankle (Fig. 6(i)) actuators, on average, can reach 12.7, 28.2 and 9.4 N m, respectively, and greatly improved the transparency of the system, as previously shown in Fig. 5.

Additional aspects of the gait kinematics are shown in Fig. 7(a), where the knee angle is displayed against the hip angle for the three sets of data collection, i.e. ExoOff, denoted by red line, ExoTransp, green line, and NoExo, gray line. Fig. 7(b) presents the heel trajectory for the same experiments. Solid lines represent the average values of the parameter, and shaded areas represent the variability computed as standard deviation. During ExoOff trials, the low backdrivability of the actuators, strongly restricts the RoM of the joint, as can be noticed by the solid red line in Fig. 7(a), and, consequently, the heel trajectory and foot clarence, thereby reducing the step length and step height, Fig. 7 (b).

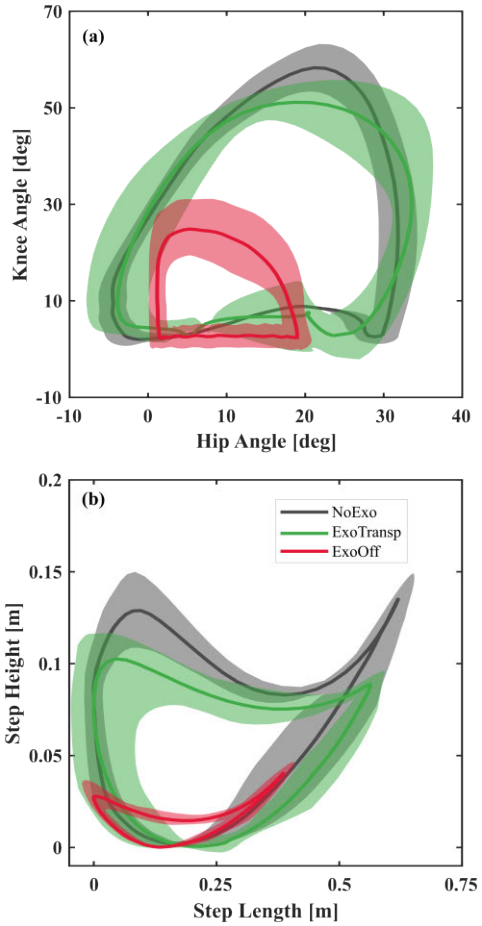

FIGURE 7. Knee angle vs. hip angle (a) and heel trajectory (b) during over-ground walking. Solid lines represent average values and shaded areas represent the variability (i.e., standard deviation). Green lines are ExoTransp, red lines are ExoOff, and solid gray lines are NoExo data.

This effect and the high torque required to move the joints, as shown in Fig. 5, prevent the user from walking normally. On the other hand, comparing the RoM and heel trajectory averages of the ExoTransp and NoExo trials, we noticed that the transparent system could greatly restore the joints RoM, foot clearance and step length, while requiring low interaction torque as previously shown.

To investigate the effect of the exoskeleton on the user's kinematics, we calculate the spatiotemporal parameters of the gait as shown in Fig. 8. For the statistical analyses * indicates $p < 0.05$, ** represents $p < 0.01$, and *** for $p < 0.001$. As previously presented, the transparent control is able to restore the spatial parameters of the gait as it can be seen in Fig. 8(a) and (b) where the stride length (SL) and step height (SH) are presented. No significant differences are observed between the ExoTransp and NoExo experiments ($p = 0.129$ for SL and $p = 0.245$ for SH). On the other hand, significant changes in SL and SH means are detected when the user walks in ExoOff and ExoTransp modes ($p = 0.045$ for SL and $p = 0.012$ for SH). However, the same trend is not detected for the cadence in Fig. 8

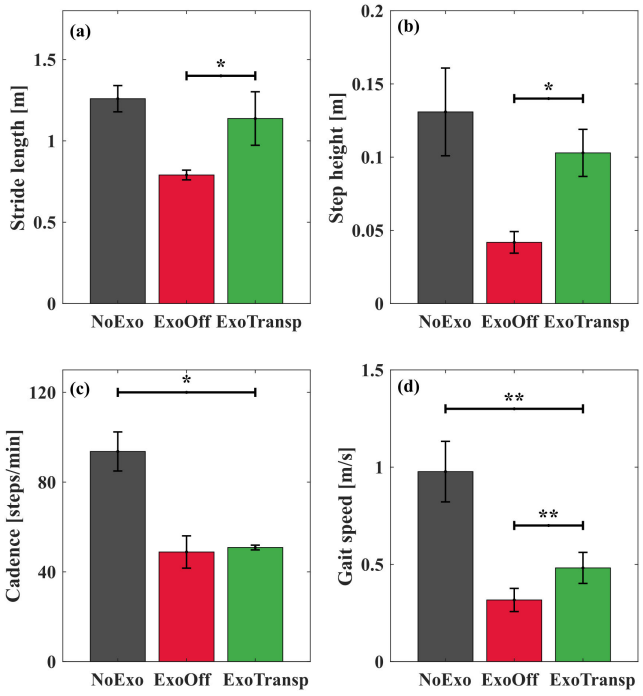

FIGURE 8. Spatiotemporal parameters of the gait cycle. (a) step length, (b) step height, (c) cadence, and (d) gait speed. Vertical bars represent the standard deviation. Asterix marks (*) represent significance level, * for $p < 0.05$ and ** for $p < 0.01$.

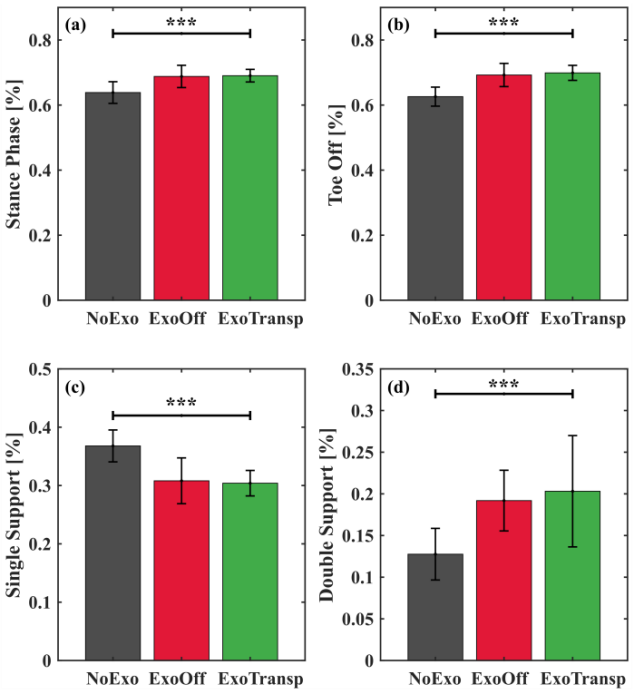

FIGURE 9. Temporal parameters as percentage of the gait cycle (%). (a) stance phase, (b) toe off, (c) single support, and (d) double support. Vertical bars represent the standard deviation, whereas asterix marks (*) represent significance level, *** for $p < 0.001$.

(c). No significant difference in stepping frequency is observed between ExoOff and ExoTransp ($p = 0.644$), but significant change among ExoTransp and NoExo ($p = 0.015$) is noticed. Finally, in all the sets of experiments (Fig. 8(d)) the gait speed is significantly different, with $p = 0.005$ for ExoOff – ExoTransp and $p = 0.008$ for ExoTransp – NoExo.

To further investigate the effect of the temporal parameters of gait, Fig. 9 presents the temporal parameters as a function of the gait cycle percentage. It is interesting to note that the stance phase parameters (%) (Fig. 9(a)), toe off (%) (Fig. 9(b)), single support (%) (Fig. 9(c)), and double support (%) (Fig. 9(d)) do not show significant differences between ExoTransp and ExoOff, with $p = 0.885$, 0.502, 0.756, and 0.420, respectively. On the other hand, the same parameters show a significant difference between NoExo and ExoTransp, with $p < 0.001$.

IV. DISCUSSION

Although human gait kinematics and kinetics appear to be quite similar when comparing treadmill and level ground walking [37], robotic-assisted GT presents important differences [2]. Unlike treadmill gait rehabilitation trainers, where subjects are supported by a harness and handrails and remain ''stationary'' therefore primarily relying on a feedforward control of lower-limb movements, during overground walking the subjects proceed along path. Participation of the subject is crucial to walk forward while maintaining stability, thus requiring closed-loop gait control [9]. Such differences make overground exoskeletons a potentially more effective tool to improve the subject's participation in the rehabilitation process [8]. For this reason, transparency becomes a key aspect of the overground GT exoskeleton.

Several previous researches sought to develop transparency strategies to improve exoskeleton's backdrivability [3], [16], [17], [18], [19], [20], [23], [24], [25], [26], [27], [28], [29], [35]. However, transparent operation remains an open problem, since the singularity of each system requires specific approaches [17], that account for the kind of actuator, number of DoF, system sensing and other factors. Previous studies explored the effects of transparent operation strategies on user kinematics for treadmill-based exoskeletons [3], [26], [27]. However, since overground GT requires greater user engagement, we investigated how a transparent exoskeleton for overground GT affects the gait kinematics and spatiotemporal parameters.

The results presented in Fig. 5 show the effectiveness of the proposed transparent controller. The exoskeleton is hardly backdrivable when unpowered, because of the high-ratio harmonic-based actuators employed to make the system lightweight and compact. The user reduced the joints RoM during walking avoiding even higher physical interaction with the robot. On the other hand, the RoM of the joints is greatly improved during transparent operation. The mean τ_{HRI} of the hip and knee joints are about 25% of the unpowered condition, whereas the joint angles are restored to the physiological condition. In other words,

IEEE Journal of Translational Engineering in Health and Medicine

the exoskeleton joints could rotate at higher velocities with lower interaction torque compared to the unpowered system. This achievement is due to the actuator and dynamic compensation and zero-torque controller, as shown in Fig. 6. The total amount of torque modulated by the transparent controller for the hip, knee, and ankle joints can reach 12.7, 28.2 and 9.4 N m, respectively, to improve the backdrivability of the system, which is remarkable. Since the level of compensation used at the ankle joint is lower than the other joints to improve stability, the difference between ExoTansp and ExoOff is less prominent. Despite the improved gait kinematics observed in Fig. 5, interestingly, the exoskeleton angles for unpowered and transparent conditions seem to be shifted to the right about 10%, representing a delayed toe-off motion.

The capacity of the transparent operation to recover the subject's kinematics is clear in Fig. 7(a) and (b). While knee and hip RoM are reduced for ExoOff, it is quite similar to the subject's physiological gait for ExoTransp. Regarding the heel trajectory, the subject displayed similar step height and stride length for both ExoTransp and NoExo walking conditions, analogous to the results in [26] using a transparent lower-limb exoskeleton while subjects walked on a treadmill. As expected, the subjects displayed lower RoM and foot clearance while walking with unpowered system. These results highlight the importance of a suitable transparent operating mode to reduce the physical interaction between the user and the exoskeleton to increase patients' active involvement during the rehabilitation process. Moreover, unlike treadmill-based GT exoskeletons [21], user gait kinematics strongly depends on the user-robot interaction during overground GT [8], [9].

Previous results demonstrated how the transparent operation mode was able to restore the gait spatial parameters operating system in lower-limb treadmill-based exoskeletons [3], [26], [27]. The plots presented in Fig. 8 and Fig. 9 highlight how a lower-limb exoskeleton can affect the user gait kinematics. In Fig. 8(a) and (b) the stride length and the step height do not show statistically significant differences between ExoTransp and NoExo ($p = 0.129$ for SL and $p = 0.245$ for SH), but show significant differences between ExoTransp and ExoOff ($p = 0.045$ for SL and $p = 0.012$ for SH). However, the temporal parameters of gait, denoted by the walking cadence (Fig. 8(c)) are not significantly different for ExoTransp and ExoOff. The subjects' stride time and cadence are significantly slower for ExoTransp and ExoOff relative to NoExo. Looking at the ExoTranp results, we observed similar stride length and step height to the ones observed for physiological gait, but the same cadence of ExoOff, thereby affecting the walking speed (Fig. 8(d)). In other words, although the joints' RoM are is restored to their physiological values with the transparent controller, the walking speed is yet significantly different for the ExoTransp and NoExo trials ($p = 0.008$). This effect cannot be noticed in treadmill-based GT systems, since the walking speed is dictated by the preselected belt speed [3], [26], [38], [39].

We speculate that the lower stepping frequency displayed by the user-exoskeleton in both ExoOff and ExoTransp conditions could be interpreted as in previous studies on attention-demanding tasks during walking [40], [41], [42]. Even though the involvement of attention in the control of the rhythmic stepping mechanism and balance during walking is not yet completely understood [41], there is evidence of reduced cadence for attention-demanding tasks during walking [40]. In a study with healthy young adults, Dubost et al. [42] noted a significant increase in stride time variability under dual-task conditions independently of walking velocity and stride length variability. Similar result is observed in ExoTransp mode relative to NoExo: no significant variation in step length and independent variation of cadence and gait speed are noticed.

Exoskeletons add mechanical impedance to the legs, change body mass and inertia distribution, and create mechanical constraints affecting the joints [43]. In this context, it is expected that walking on level ground with an exoskeleton requires more attention to properly recruit auxiliary muscles of the trunk and leg to maintain stability. In previous work [21] we investigated how the inertia, mass and friction of the exoskeleton can affect the user-robot interaction torque and lead to changes in stride time to reduce the metabolic cost of gait. Stride time increases as exoskeleton inertia, mass, and friction increase [38], [39]. However, since the exoskeleton dynamics is modified by the transparent controller, and the cadence of ExoTransp and ExoOff are not statistically different ($p = 0.644$), the reduced stepping frequency observed here are independently of user-robot interaction torques. Cajigas et al. [44] suggested that motor adaptation generated by the central nervous system (CNS) in response to forces exerted by a robot is primarily driven by locomotor stability, secondarily by energy expenditure, and only lastly to preserve the walking pattern. This work provides further evidence that the dynamics of the user's leg is modified by the exoskeleton suggesting that the CNS identifies it as a relevant task to preserve balance, possibly leading the user to reduce cadence. Although the transparent controller is able to substantially reduce the mechanical impedance added to the user's legs, this strategy is not enough to avoid interfering with the user balance and change the walking pattern.

The results presented here are quite distinct from those in [3], [27], and [38], where the authors investigated transparency in treadmill-based exoskeletons. These authors observed a decrease in cadence associated with an increase in step length compared to free walking at the same treadmill speed. Unlike overground exoskeletons, in treadmill-based GT, user balance is preserved by bodyweight support and handrails in addition to a constant gait speed provided by the walking belt. In this scenario, changes in gait characteristics might be driven by gait energetic expenditure, when balance is not challenged [44]. The modified inertia distribution of the user's legs leads to an increase in step length [38], [39], which results in a lower cadence for the same belt speed [21].

Finally, delayed toe-off and increased double support results as presented in Fig. 9 for both ExoTransp and ExoOff are related to increased stride time and possibly the extra attention required by the user to maintain balance while walking with the exoskeleton. These results are also supported by previous studies with focus on attention-demanding tasks during walking [40], [41], [42]. The reduced swing period, denoted by the single support phase (Fig. 9(c)) provides further evidence that increased stride time is not related to the added inertia to the user limbs [39]. These results support the hypothesis that the user reduces stepping frequency to improve locomotor stability while walking with the exoskeleton. The results shown here point out that the transparent control method applied to lower-limb overground walking exoskeletons must go further than to reduce the impedance of the system in the user's legs, it needs to address users' dynamic stability. Moreover, gait training protocols for overground lower-limb exoskeletons should consider potential changes in cadence, gait speed, and other spatiotemporal parameters, while the user is wearing the exoskeleton, before these parameters are set for the training session. As gait training should improve locomotor stability [44], [45] and walking at an unnatural stepping frequency is expected to impact locomotor stability, gait spatiotemporal parameters should be carefully examined to assure positive outcomes of exoskeleton-assisted gait rehabilitation.

This study presents some limitations that are important to highlight. First, statistical analysis of the results would benefit from a larger population of subjects. Additionally, due to the space limitations of our experimental setup we did not evaluate the use of the exoskeleton for long periods of linear walking, limiting our ability to evaluate more characteristics and behaviors associated with motor adaptation. Finally, changes in spatiotemporal parameters may emerge once users become more familiar with the exoskeleton after long periods of use. However, the experimental protocol designed for this study did not allow us to assess the effects of extended use of the exoskeleton. Future studies are needed to assess the effects of a transparent lower-limb exoskeleton on the gait kinematics of impaired subjects and better investigate the effects of cadence, gait speed, and other parameters when the exoskeleton is used as AAN GT system.

V. CONCLUSION

We explored the effects of the ExoRoboWalker, a six DoF overground GT exoskeleton, on the user's gait using a transparent operation controller. The designed controller comprises a feedback zero-torque controller associated with two feedforward blocks to cancel the effects of the exoskeleton's dynamics and the actuator's impedance. Compared to the ExoOff experiments, the transparent controller was able to greatly reduce user-robot interaction torques and restore the spatial parameters of the user's gait to normal walking. The walking cadence was not significantly different between the ExoOff and ExoTransp trials ($p = 0.644$). The results suggest that walking with a lower-limb exoskeleton on level ground, regardless of the transparency of the system, has an impact on subject's gait in a way that is similar to that of an attention-demanding task and affects the control of balance. In other words, it appears that subjects walking with an exoskeleton, even in transparent operation, adjust their stepping frequency to improve their dynamic stability. These outcomes have important implications for the design of gait rehabilitation protocols using lower-limb exoskeletons. Cadence, gait speed and other gait parameters should be better investigated when using overground GT exoskeletons before they are utilized as an AAN GT system, something that we intend to explore in future works.

REFERENCES

[1] R. Baud, A. R. Manzoori, A. Ijspeert, and M. Bouri, "Review of control strategies for lower-limb exoskeletons to assist gait," *J. NeuroEng. Rehabil.*, vol. 18, no. 1, p. 119, Jul. 2021, doi: 10.1186/s12984-021-00906-3.

[2] I. Díaz, J. J. Gil, and E. Sánchez, "Lower-limb robotic rehabilitation: Literature review and challenges," *J. Robot.*, vol. 2011, pp. 1–11, Nov. 2011, doi: 10.1155/2011/759764.

[3] D. Zanotto, T. Lenzi, P. Stegall, and S. K. Agrawal, "Improving transparency of powered exoskeletons using force/torque sensors on the supporting cuffs," in *Proc. IEEE 13th Int. Conf. Rehabil. Robot. (ICORR)*, Jun. 2013, pp. 1–6.

[4] A. Tsukahara, R. Kawanishi, Y. Hasegawa, and Y. Sankai, "Sit-to-stand and stand-to-sit transfer support for complete paraplegic patients with robot suit HAL," *Adv. Robot.*, vol. 24, no. 11, pp. 1615–1638, Jan. 2010, doi: 10.1163/016918610X512622.

[5] K. A. Strausser and H. Kazerooni, "The development and testing of a human machine interface for a mobile medical exoskeleton," in *Proc. IEEE/RSJ Int. Conf. Intell. Robots Syst.*, Sep. 2011, pp. 4911–4916, doi: 10.1109/IROS.2011.6095025.

[6] T. Yan, M. Cempini, C. M. Oddo, and N. Vitiello, "Review of assistive strategies in powered lower-limb orthoses and exoskeletons," *Robot. Auto. Syst.*, vol. 64, pp. 120–136, Feb. 2015, doi: 10.1016/j.robot.2014.09.032.

[7] I. Borggraefe et al., "Robotic-assisted treadmill therapy improves walking and standing performance in children and adolescents with cerebral palsy," *Eur. J. Paediatric Neurol.*, vol. 14, no. 6, pp. 496–502, Nov. 2010, doi: 10.1016/j.ejpn.2010.01.002.

[8] S. A. Murray, K. H. Ha, C. Hartigan, and M. Goldfarb, "An assistive control approach for a lower-limb exoskeleton to facilitate recovery of walking following stroke," *IEEE Trans. Neural Syst. Rehabil. Eng.*, vol. 23, no. 3, pp. 441–449, May 2015, doi: 10.1109/TNSRE.2014.2346193.

[9] M. Bortole et al., "The H2 robotic exoskeleton for gait rehabilitation after stroke: Early findings from a clinical study," *J. NeuroEng. Rehabil.*, vol. 12, no. 1, p. 54, Jun. 2015.

[10] S. Horton, K. Mares, N. Coull, and F. Poland, "On the character and production of 'active participation' in neuro-rehabilitation: An actor-network perspective," *Sociol. Health Illness*, vol. 39, no. 8, pp. 1529–1541, Nov. 2017, doi: 10.1111/1467-9566.12615.

[11] W. Huo, S. Mohammed, J. C. Moreno, and Y. Amirat, "Lower limb wearable robots for assistance and rehabilitation: A state of the art," *IEEE Syst. J.*, vol. 10, no. 3, pp. 1068–1081, Sep. 2016.

[12] F. el Zahraa Wehbi, W. Huo, Y. Amirat, M. E. Rafei, M. Khalil, and S. Mohammed, "Active impedance control of a knee-joint orthosis during swing phase," in *Proc. Int. Conf. Rehabil. Robot. (ICORR)*, Jul. 2017, pp. 435–440.

[13] G. Aguirre-Ollinger, J. E. Colgate, M. A. Peshkin, and A. Goswami, "Active-impedance control of a lower-limb assistive exoskeleton," in *Proc. IEEE 10th Int. Conf. Rehabil. Robot.*, Jun. 2007, pp. 188–195.

[14] R. M. Andrade, S. Sapienza, E. E. Fabara, and P. Bonato, "Trajectory tracking impedance controller in 6-DoF lower-limb exoskeleton for over-ground walking training: Preliminary results," in *Proc. Int. Symp. Med. Robot. (ISMR)*, Nov. 2021, pp. 1–6, doi: 10.1109/ISMR48346.2021.9661558.

[15] A. Ajoudani, "Teleimpedance based assistive control for a compliant knee exoskeleton," in *Transferring Human Impedance Regulation Skills to Robots*, A. Ajoudani, Ed. Cham, Switzerland: Springer, 2016, pp. 119–138, doi: 10.1007/978-3-319-24205-7_9.

[16] R. Mendoza-Crespo, R. Soto, and J. L. Pons, "Transparent mode for lower limb exoskeleton," in *Wearable Robotics: Challenges Trends* (Biosystems & Biorobotics), vol. 16. 2017, pp. 421–425. [Online]. Available: https://link.springer.com/chapter/10.1007/978-3-319-46532-6_69

[17] R. M. Andrade, S. Sapienza, and P. Bonato, "Development of a 'transparent operation mode' for a lower-limb exoskeleton designed for children with cerebral palsy," in *Proc. IEEE 16th Int. Conf. Rehabil. Robot. (ICORR)*, Jun. 2019, pp. 512–517, doi: 10.1109/ICORR.2019.8779432.

[18] Y. Zhang, K. J. Nolan, and D. Zanotto, "Oscillator-based transparent control of an active/semiactive ankle-foot orthosis," *IEEE Robot. Autom. Lett.*, vol. 4, no. 2, pp. 247–253, Apr. 2019, doi: 10.1109/LRA.2018.2886400.

[19] R. M. Andrade, P. H. F. Ulhoa, and C. B. S. Vimieiro, "Designing a highly backdrivable and kinematic compatible magneto-rheological knee exoskeleton," in *Proc. Int. Conf. Robot. Autom. (ICRA)*, May 2022, pp. 5724–5730, doi: 10.1109/ICRA46639.2022.9812308.

[20] T. Elery, S. Rezazadeh, C. Nesler, and R. D. Gregg, "Design and validation of a powered Knee–Ankle prosthesis with high-torque, low-impedance actuators," *IEEE Trans. Robot.*, vol. 36, no. 6, pp. 1649–1668, Dec. 2020, doi: 10.1109/TRO.2020.3005533.

[21] R. M. Andrade and P. Bonato, "The role played by mass, friction, and inertia on the driving torques of lower-limb gait training exoskeletons," *IEEE Trans. Med. Robot. Bionics*, vol. 3, no. 1, pp. 125–136, Feb. 2021, doi: 10.1109/TMRB.2021.3052014.

[22] R. M. Andrade, A. B. Filho, C. B. S. Vimieiro, and M. Pinotti, "Optimal design and torque control of an active magnetorheological prosthetic knee," *Smart Mater. Struct.*, vol. 27, no. 10, Sep. 2018, Art. no. 105031, doi: 10.1088/1361-665X/aadd5c.

[23] C. Véronneau, J.-P. L. Bigué, A. Lussier-Desbiens, and J.-S. Plante, "A high-bandwidth back-drivable hydrostatic power distribution system for exoskeletons based on magnetorheological clutches," *IEEE Robot. Autom. Lett.*, vol. 3, no. 3, pp. 2592–2599, Jul. 2018, doi: 10.1109/LRA.2018.2812910.

[24] R. M. de Andrade, P. H. F. Ulhoa, E. A. F. Dias, A. B. Filho, and C. B. S. Vimieiro, "Design and testing a highly backdrivable and kinematic compatible magneto-rheological knee exoskeleton," *J. Intell. Mater. Syst. Struct.*, vol. 34, no. 6, pp. 653–663, Apr. 2023, doi: 10.1177/1045389X221117496.

[25] P. Stegall, K. Winfree, D. Zanotto, and S. K. Agrawal, "Rehabilitation exoskeleton design: Exploring the effect of the anterior lunge degree of freedom," *IEEE Trans. Robot.*, vol. 29, no. 4, pp. 838–846, Aug. 2013, doi: 10.1109/TRO.2013.2256309.

[26] V. Bartenbach, D. Wyss, D. Seuret, and R. Riener, "A lower limb exoskeleton research platform to investigate human-robot interaction," in *Proc. IEEE Int. Conf. Rehabil. Robot. (ICORR)*, Aug. 2015, pp. 600–605, doi: 10.1109/ICORR.2015.7281266.

[27] H. Vallery, A. Duschau-Wicke, and R. Riener, "Generalized elasticities improve patient-cooperative control of rehabilitation robots," in *Proc. IEEE Int. Conf. Rehabil. Robot.*, Jun. 2009, pp. 535–541, doi: 10.1109/ICORR.2009.5209595.

[28] X. Chen, Y. Zeng, and Y. Yin, "Improving the transparency of an exoskeleton knee joint based on the understanding of motor intent using energy kernel method of EMG," *IEEE Trans. Neural Syst. Rehabil. Eng.*, vol. 25, no. 6, pp. 577–588, Jun. 2017, doi: 10.1109/TNSRE.2016.2582321.

[29] M. J. Claros, R. Soto, J. L. Gordillo, J. L. Pons, and J. L. Contreras-Vidal, "Robotic assistance of human motion using active-backdrivability on a geared electromagnetic motor," *Int. J. Adv. Robotic Syst.*, vol. 13, no. 2, p. 40, Mar. 2016.

[30] B. Hwang and D. Jeon, "A method to accurately estimate the muscular torques of human wearing exoskeletons by torque sensors," *Sensors*, vol. 15, no. 4, pp. 8337–8357, Apr. 2015.

[31] J.-P. Hauschild and G. R. Heppler, "Control of harmonic drive motor actuated flexible linkages," in *Proc. IEEE Int. Conf. Robot. Autom.*, Apr. 2007, pp. 3451–3456.

[32] S. Murray and M. Goldfarb, "Towards the use of a lower limb exoskeleton for locomotion assistance in individuals with neuromuscular locomotor deficits," in *Proc. Conf. IEEE Eng. Med. Biol. Soc.*, Aug. 2012, pp. 1912–1915.

[33] M. R. Kermani, R. V. Patel, and M. Moallem, "Friction identification and compensation in robotic manipulators," *IEEE Trans. Instrum. Meas.*, vol. 56, no. 6, pp. 2346–2353, Dec. 2007.

[34] R. M. de Andrade, J. S. R. Martins, M. Pinotti, A. B. Filho, and C. B. S. Vimieiro, "Novel active magnetorheological knee prosthesis presents low energy consumption during ground walking," *J. Intell. Mater. Syst. Struct.*, vol. 32, no. 14, pp. 1591–1603, Jan. 2021, doi: 10.1177/1045389X20983923.

[35] T. Nef and P. Lum, "Improving backdrivability in geared rehabilitation robots," *Med. Biol. Eng. Comput.*, vol. 47, no. 4, pp. 441–447, Apr. 2009.

[36] J. Sergey, S. Sergei, and Y. Andrey, "Comparative analysis of global optimization-based controller tuning methods for an exoskeleton performing push recovery," in *Proc. 20th Int. Conf. Syst. Theory, Control Comput. (ICSTCC)*, Oct. 2016, pp. 107–112, doi: 10.1109/ICSTCC.2016.7790649.

[37] P. O. Riley, G. Paolini, U. Della Croce, K. W. Paylo, and D. C. Kerrigan, "A kinematic and kinetic comparison of overground and treadmill walking in healthy subjects," *Gait Posture*, vol. 26, no. 1, pp. 17–24, Jun. 2007, doi: 10.1016/j.gaitpost.2006.07.003.

[38] X. Jin, Y. Cai, A. Prado, and S. K. Agrawal, "Effects of exoskeleton weight and inertia on human walking," in *Proc. IEEE Int. Conf. Robot. Autom. (ICRA)*, May 2017, pp. 1772–1777.

[39] D. Zanotto, Y. Akiyama, P. Stegall, and S. K. Agrawal, "Knee joint misalignment in exoskeletons for the lower extremities: Effects on user's gait," *IEEE Trans. Robot.*, vol. 31, no. 4, pp. 978–987, Aug. 2015.

[40] O. Beauchet, V. Dubost, F. R. Herrmann, and R. W. Kressig, "Stride-to-stride variability while backward counting among healthy young adults," *J. NeuroEng. Rehabil.*, vol. 2, no. 1, p. 26, Aug. 2005, doi: 10.1186/1743-0003-2-26.

[41] V. Dubost et al., "Relationships between dual-task related changes in stride velocity and stride time variability in healthy older adults," *Hum. Movement Sci.*, vol. 25, no. 3, pp. 372–382, Jun. 2006, doi: 10.1016/j.humov.2006.03.004.

[42] V. Dubost, C. Annweiler, K. Aminian, B. Najafi, F. R. Herrmann, and O. Beauchet, "Stride-to-stride variability while enumerating animal names among healthy young adults: Result of stride velocity or effect of attention-demanding task?" *Gait Posture*, vol. 27, no. 1, pp. 138–143, Jan. 2008, doi: 10.1016/j.gaitpost.2007.03.011.

[43] S. Rossi, A. Colazza, M. Petrarca, E. Castelli, P. Cappa, and H. I. Krebs, "Feasibility study of a wearable exoskeleton for children: Is the gait altered by adding masses on lower limbs?" *PLoS ONE*, vol. 8, no. 9, Sep. 2013, Art. no. e73139.

[44] I. Cajigas, A. Koenig, G. Severini, M. Smith, and P. Bonato, "Robot-induced perturbations of human walking reveal a selective generation of motor adaptation," *Sci. Robot.*, vol. 2, no. 6, May 2017, Art. no. eaam7749.

[45] T. Mikolajczyk, "Advanced technology for gait rehabilitation: An overview," *Adv. Mech. Eng.*, vol. 10, no. 7, Jul. 2018, Art. no. 1687814018783627, doi: 10.1177/1687814018783627.